Anal. Chem. **2007,** *79,* 7965−7974

Accelerated Articles

Resolving Oligomers from Fully Grown Polymers with IMS−MS

Sarah Trimpin, Manolo Plasencia, Dragan Isailovic, and David E. Clemmer*

Department of Chemistry, Indiana University, Bloomington, Indiana 47405

Ion mobility and mass spectrometry techniques, combined with electrospray ionization, have been used to examine distributions of poly(ethylene glycols) (PEG) with average molecular masses of 6550 and 17900 Da. The analysis provides information about the polymer size distributions as well as smaller oligomers existing over a wide range of charge states and sizes (i.e., $[HO(CH_2CH_2O)_xH + nCs]^{n+}$, where x ranges from 21 to 151 and $n = 2$ to 11 for the 6550 Da sample; and, x ranges from 21 to 362 and $n = 2$ to 23 for the 17 900 Da sample). The present data show that oligomer distributions also fall into families, corresponding to much narrower size distributions for individual charge states; this dramatically simplifies data analysis. For example, we show evidence for baseline resolution of the +10 charge state of polymers. Unlike the charge-state trends reported previously for peptide ion families, which show generally increasing mobilities with increasing charge state (for a given m/z value), the mobilities of $[HO(CH_2CH_2O)_xH + nCs]^{n+}$ families generally decrease with increasing charge state. This requires that the addition of charges leads to substantial changes in the average structures of the ions. Comparisons of cross section calculations from molecular modeling results for multiply cesiated PEG ions with experimental cross sections indicate that these ions adopt highly extended (in many cases nearly linear) conformations, except for the high degree of coordination of the charged sites.

Synthetic polymers are used ubiquitously across a wide range of industries (e.g., chemical, pharmaceutical, and manufacturing) and are, therefore, of significant interest.[1−3] Such compounds are described by indication of the monomer unit composition and a value that represents the average size or molecular weight [e.g., poly(ethylene glycol) (PEG) 6550, which corresponds to a polymeric ethylene oxide chain containing ∼150 monomer units]. Historically, methods aimed at characterizing polymers (e.g., light scattering or size exclusion chromatography)[4] only provide information about the bulk material. However, it is generally understood that even simple polymers created from well-characterized reactions may exist as a mixture of sizes commonly defined by the polydispersity index (PDI).[4] If more complex chemistries are employed, significant chemical heterogeneity may also be present, such as variations in end-groups or within the polymer chain (e.g., copolymers).

* To whom the correspondence should be addressed. E-mail: clemmer@indiana.edu.

(1) Pino, P.; Mülhaupt, R. *Angew. Chem., Int. Ed. Engl.* **1980**, *19*, 857−875. Wegner, G. *Angew. Chem., Int. Ed. Engl.* **1981**, *20*, 361−381. Gros, L.; Ringsdorf, H.; Schupp, H. *Angew. Chem., Int. Ed. Engl.* **1981**, *20*, 305−325. Bader, H.; Ringsdorf, H.; Schmidt, B. *Angew. Makromol. Chem.* **1984**, *123*, 457−485. Ringsdorf, H.; Schlarb, B.; Venzmer, J. *Angew. Chem., Int. Ed. Engl.* **1988**, *27*, 113−158. Brintzinger, H. H.; Fischer, D.; Mülhaupt, R.; Rieger, B.; Waymouth, R. M. *Angew. Chem., Int. Ed. Engl.* **1995**, *34*, 1143−1170. Kraft, A.; Grimsdale, A. C.; Holmes, A. B. *Angew. Chem., Int. Ed. Engl.* **1998**, *37*, 402−428. Scherf, U.; List, E. J. W. *Adv. Mater.* **2002**, *14*, 477−487. Ringsdorf, H. *Angew. Chem., Int. Ed.* **2004**, *43*, 1064−1076. Duncan, R.; Ringsdorf, H.; Satchi-Fainaro, R. *Adv. Polym. Sci.* **2006**, *192*, 1−8.

(2) Räder, H. J.; Schrepp, W. *Acta Polym.* **1998**, *49*, 272−293. Hanton, S. D. *Chem. Rev.* **2001**, *101*, 527−569. Montaudo, G.; Samperi, F.; Montaudo, M. S. *Prog. Polym. Sci.* **2006**, *31*, 277−357.

(3) Setayesh, S.; Grimsdale, A. C.; Weil, T.; Enkelmann, V.; Müllen, K.; Meghdadi, F.; List, E. J. W.; Leising, G. *J. Am. Chem. Soc.* **2001**, *123*, 946−953. Peacock, P. M.; McEwen, C. N. *Anal. Chem.* **2006**, *78*, 3957−3964.

(4) Dawkins, J. V. *Pure Appl. Chem.* **1982**, *54*, 281−292. Hamielec, A. *Pure Appl. Chem.* **1982**, *54*, 293−307. Gaborieau, M.; Gilbert, R. G.; Gray-Weale, A.; Hernandez, J. M.; Castignolles, P. *Macromol. Theory Simul.* **2007**, *16*, 13−28.

(5) Fenn, J. B.; Mann, M.; Meng, C. K.; Wong, S. F.; Whitehouse, C. M. *Science* **1989**, *246*, 64−67.

10.1021/ac071575i CCC: $37.00
Published on Web 09/22/2007

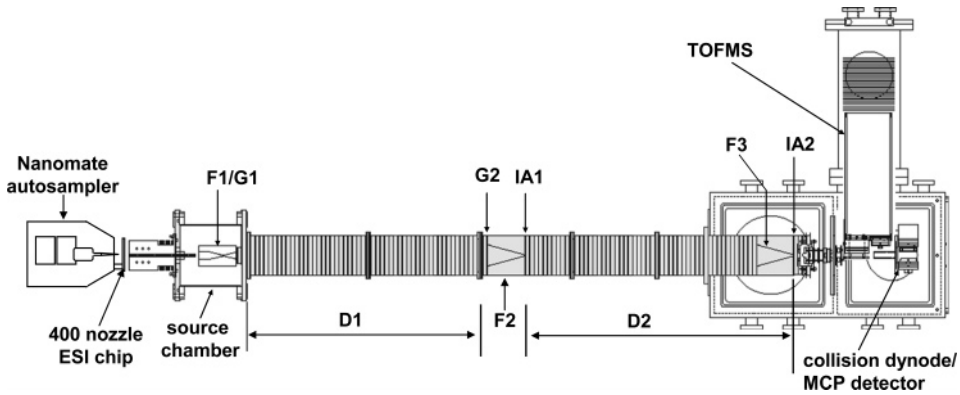

Figure 1. Schematic diagram of the ESI-IMS−IMS−MS instrument. Ions accumulated in the source funnel (F1) are gated through ion gate G1, where they undergo mobility separation in consecutive drift regions (D1, D2). Ions can be selected on the basis of mobility at G2 and used to determine cross sections. Samples are infused into the source region by means of a Nanomate autosampler mounted at the ESI source. For more detail on ion selection and cross section determination, refer to the text.

Soft ionization methods such as electrospray ionization (ESI)[5] and matrix-assisted laser desorption/ionization (MALDI),[6] combined with mass spectrometry (MS), make it possible to examine polymeric systems in detail, such that the individual sizes and different compositions may often be delineated.[2,3,7−10] From its inception, ESI-MS has provided an especially interesting approach to polymer analysis. In 1988, Fenn and co-workers[11] examined a range of PEG sizes and showed that it was possible to detect 17.5 kDa species using an instrument with an upper mass-to-charge (m/z) limit of 1500, a result of the multiple charging phenomenon associated with ESI. This same phenomenon limits the ability to resolve individual components in a mixture. That is, the charge-state distribution is often convoluted over the size distribution resulting in many isobaric ions and broad mass spectral features. A number of methods have been used to address these ESI-related issues, including: methods for reducing the PDI by employing techniques such as gel-permeation chromatography;[12] removal of charge carriers from ions in order to reduce complexity associated with multiple charging,[13] and incorporation of higher resolution MS approaches such as Fourier transform (FT) MS in order to resolve isotopic spacing of multiply charged species.[14]

Here, we examine the utility of a combination of ESI with ion mobility spectrometry (IMS) and MS for characterizing polymeric systems by studying PEG (6550 and 17 900 Da). The results show that inclusion of an IMS dimension is highly complementary to MS for such analyses. As reported for other biopolymers,[15−19] ions fall into families depending upon their sizes and charge states. Interestingly, in the present work, we find that PEG families are distinctly different from any we have measured previously because the average mobility of the families decreases with increasing charge state. The analysis makes it possible to see a range of low-abundance oligomers that would normally be hidden in the background if only MS was used for analysis, including families of isobaric species that are readily resolved by IMS−MS.

The present work provides insight about ion structures and is therefore closely related to ion mobility measurements of smaller cesiated PEG ions $[HO(CH_2CH_2O)_xH + Cs]^+$ produced by

(6) Tanaka, K.; Waki, H.; Ido, Y.; Akita, S.; Yoshida, Y.; Yoshida, T. *Rapid Commun. Mass Spectrom.* **1988**, *2*, 151−153. Karas, M.; Hillenkamp, F. *Anal. Chem.* **1988**, *60*, 2299−2301.
(7) Räder, H. J.; Spickermann, J.; Kreyenschmidt, M. M.; Müllen, K. *Macromol. Chem. Phys.* **1996**, *197*, 3285−3296. Räder, H. J.; Spickermann, J.; Müllen, K. *Macromol. Chem. Phys.* **1996**, *196*, 3967−3978. Trimpin, S.; Rouhanipour, A.; Az, R.; Räder, H. J.; Müllen, K. *Rapid Commun. Mass Spectrom.* **2001**, *15*, 1364−1373. Trimpin, S.; Grimsdale, A. C.; Räder, H. J.; Müllen, K. *Anal. Chem.* **2002**, *74*, 3777−3782. Trimpin, S.; McEwen, C. N. *J. Am. Soc. Mass Spectrom.* **2007**, *18*, 377−381.
(8) Martin, K.; Spickermann, J.; Räder, H. J.; Müllen, K. *Rapid Commun. Mass Spectrom.* **1996**, *10*, 1471−1474. Trimpin, S.; Eicchorn, P.; Räder, H. J.; Müllen, K.; Knepper, T. P. *J. Chromatogr., A* **2001**, *938*, 67−77. Trimpin, S.; Keune, S.; Räder, H. J.; Müllen, K. *J. Am. Mass Spectrom.* **2006**, *17*, 661−671.
(9) Rittig, F.; Fandrich, N.; Melanie, U.; Schrepp, W.; Just, U.; Weidner, S. M. *Macromol. Chem. Phys.* **2006**, *207*, 1026−1037. Weidner, S.; Falkenhagen, J.; Krueger, R. P.; Just, U. *Anal. Chem.* **2007**, *79*, 4814−4819. Trimpin, S.; Weidner, S. M.; Falkenhagen, J.; McEwen, C. N. *Anal. Chem.* **2007**, *79*, 7565−7570.
(10) McEwen, C. N.; Simonsick, W. J.; Larsen, B. S.; Ute, K.; Hatada, K. *J. Am. Soc. Mass Spectrom.* **1995**, *6*, 906−911. Jackson, A. T.; Slade, S. E.; Scrivens, J. H. *Int. J. Mass Spectrom.* **2004**, *238*, 265−277.
(11) Wong, S. F.; Meng, C. K.; Fenn, J. B. *J. Phys. Chem.* **1988**, *92*, 546−550.
(12) Aaserud, D. J.; Prokai, L.; Simonsick, W. J. *Anal. Chem.* **1999**, *71*, 4793−4799.
(13) Cody, R. B.; Tamura, J.; Musselman, B. D. *Anal. Chem.* **1992**, *64*, 1561−1570. Stephenson, J. L.; McLuckey, S. A. *J. Am. Soc. Mass Spectrom.* **1998**, *9*, 957−965. Kaufman, S. L.; Skogen, J. W.; Dorman, F. D.; Zarrin, F.; Lewis, L. C. *Anal. Chem.* **1996**, *68*, 1895−1904. Saucy, D. A.; Ude, S.; Lenggoro, I. W.; de la Mora, J. F. *Anal. Chem.* **2004**, *76*, 1045−1053. Lennon, J. D.; Cole, S. P.; Glish, G. L. *Anal. Chem.* **2006**, *78*, 8472−8476.
(14) O'Connor, P. B.; McLafferty, F. W. *J. Am. Chem. Soc.* **1995**, *117*, 12826−12831.
(15) Valentine, S. J.; Counterman, A. E.; Hoaglund, C. S.; Reilly, J. P.; Clemmer, D. E. *J. Am. Soc. Mass Spectrom.* **1998**, *9*, 1213−1216.
(16) Pringle, S. D.; Giles, K.; Wildgoose, J. L.; Williams, J. P.; Slade, S. E.; Thalassinos, K.; Bateman, R. H.; Bowers, M. T.; Scrivens, J. H. *Int. J. Mass Spectrom.* **2007**, *261*, 1−12.
(17) Counterman, A. E.; Clemmer, D. E. *J. Am. Chem. Soc.* **2001**, *123*, 1490−1498. Counterman, A. E.; Hilderbrand, A. E.; Srebalus Barnes, C. A.; Clemmer, D. E. *J. Am. Soc. Mass Spectrom.* **2001**, *12*, 1020−1035. Counterman, A. E.; Clemmer, D. E. *J. Phys. Chem. B* **2004**, *108*, 4885−4898. Matz, L. M.; Asbury, G. R.; Hill, H. H. *Rapid Commun. Mass Spectrom.* **2002**, *16*, 670−675. Woods, A. S.; Ugarov, M.; Egan, T.; Koomen, J.; Gillig, K. J.; Fuhrer, K.; Gonin, M.; Schultz, J. A. *Anal. Chem.* **2004**, *76* (8), 2187−2195. Ruotolo, B. T.; McLean, J. A.; Gillig, K. J.; Russell, D. H. *J. Am. Soc. Mass Spectrom.* **2005**, *16*, 158−165.
(18) Hoaglund-Hyzer, C. S.; Lee, Y. J.; Counterman, A. E.; Clemmer, D. E. *Anal. Chem.* **2002**, *74*, 992−1006.
(19) Henderson, S. C.; Valentine, S. J.; Counterman, A. E.; Clemmer, D. E. *Anal. Chem.* **1999**, *71*, 291−301.

MALDI[20,21] as well as protonated[22] and ammoniated[23] PEG ions generated by ESI. By comparing mobilities calculated for trial conformations with those obtained from their experiment, Bowers et al.[20,21] gained insight about the coordination of these ions by small oligomers. De la Mora and co-workers[23] found evidence for linear polymer structures based on differential mobility measurements.

EXPERIMENTAL SECTION

General Information. Figure 1 shows a schematic diagram of one of two similar drift tube mass spectrometers used for these studies. Detailed descriptions of these[24−28] and other IMS instruments,[29] as well as associated IMS theory,[20,30−32] are published elsewhere;[18,33] below, we provide only a limited overview of the experimental sequence used to make measurements, the instrumental design and capabilities, and methods used for obtaining insight about structure.

Experimental Sequence for Separating Polymer Ions. A continuous beam of ions is produced by ESI and accumulated in an ion funnel. Periodically, an electrostatic gate at the end of the funnel is lowered, allowing a short pulse of ions to enter a drift region that is filled with He buffer gas. Ions drift across this region under the influence of a field and separate according to differences in mobility. For a given charge state, compact ions (with relatively small collision cross sections) will have higher mobilities than extended structures (having larger cross sections). As ions exit the drift tube, they are focused into the source of a time-of-flight (TOF) mass spectrometer and detected. Flight times in the evacuated mass spectrometer are much shorter than drift times through the buffer gas; therefore, it is possible to record data in a nested fashion as described previously.[18,34]

IMS−IMS−MS Instrument Description. The instrument in Figure 1 incorporates two consecutive drift tubes that are each ∼1 m in length. A second instrument used to record some of the data shown here is analogous except that it incorporates three 1-m-long drift tubes. In addition to the two drift regions (D1, D2) the instrument incorporates three ion funnels (F1, F2, F3), two ion gates (G1, G2), and two ion activation regions (IA1, IA2) as labeled in the figure. The instrument can be operated in several different modes.[24,25,27] Nested IMS−MS data sets are recorded by operating all drift regions and the funnels (F2, F3) in transmission mode as described. It is also possible to select ions of specified mobilities at G2 as well as activate ions in the activation regions (also described in detail previously).[24] We use selections of specific ions at G2 in order to determine collision cross sections.[24] Ion activation inside the drift tube also appears to improve the ability to resolve some components.

Ion Funnels and Drift Regions. Key to the use of long drift tubes is prevention of ion losses; ion transmission is increased by inclusion of an ion funnel, similar in design to that developed by Smith and co-workers.[35] Funnel F1 is located at the entrance to the drift tube and functions to improve ion transmission and provides a means of accumulating the continuous ESI beam for pulsed experiments. The funnels F2 and F3 are used to focus diffuse ion clouds back onto the axis of the drift tube; effectively this configuration makes high transmission, long drift tube designs possible.[25−28] Additionally, the funnels provide a natural boundary between drift regions. The entire assembly is ∼2 m long, where drift regions D1 is ∼94 cm, D2 is ∼100 cm, and D3 is ∼95 cm. The drift regions are typically operated at ∼8−11 V cm^{-1}. The axial fields of the funnels are operated at ∼9−10 V cm^{-1}. Three rf generators built in-house provide voltage to the ion funnels at 60 V_{p-p} (450−480 kHz). All experiments are carried out using ∼2.5 Torr of He buffer gas at ∼298 K. The pressure is determined by a Baratron capacitance manometer, and the temperature is taken to be that of the laboratory.

(20) Wyttenbach, T.; von Helden, G.; Bowers, M. T. *Int. J. Mass Spectrom.* **1997**, *165*, 377−390.

(21) Gidden, J.; Wyttenbach, T.; Jackson, A. T.; Scrivens, J. H.; Bowers, M. T. *J. Am. Chem. Soc.* **2000**, *122*, 4692−4699.

(22) Robinson, E. W.; Sellon, R. E.; Williams, E. R. *Int. J. Mass Spectrom.* **2007**, *259*, 87−95.

(23) Ude, S.; de la Mora, J. F.; Thomson, B. A. *J. Am. Chem. Soc.* **2004**, *126*, 12184−12190.

(24) Merenbloom, S. I.; Koeniger, S. L.; Valentine, S. J.; Plasencia, M. D.; Clemmer, D. E. *Anal. Chem*. **2006**, *78*, 2802−2809.

(25) Koeniger, S. L.; Merenbloom, S. I.; Valentine, S. J.; Jarrold, M. F.; Udseth, H.; Smith, R.; Clemmer, D. E. *Anal. Chem.* **2006**, *78*, 4161−4174.

(26) Koeniger, S. L.; Merenbloom, S. I.; Sevugarajan, S.; Clemmer, D. E. *J. Am. Chem. Soc.* **2006**, *128*, 11713−11719.

(27) Merenbloom, S. I.; Bohrer, B. C.; Koeniger, S. L. *Anal. Chem.* **2007**, *79*, 515−522.

(28) Koeniger, S. L.; Clemmer, D. E. *J. Am. Soc. Mass Spectrom.* **2007**, *18*, 322−331.

(29) Kemper, P. R.; Bowers, M. T. *J. Am. Soc. Mass Spectrom.* **1990**, *1*, 197−207. von Helden, G.; Wyttenbach, T.; Bowers, M. T. *Int. J. Mass Spectrom. Ion Processes* **1995**, *146/147*, 349−364. Gillig, K. J.; Ruotolo, B.; Stone, E. G.; Russell, D. H.; Fuhrer, K.; Gonin, M.; Schultz, A. J. *Anal. Chem.* **2000**, *72*, 3965−3971. Cooks, R. G.; Ast, T.; Mabud, A. *Int. J. Mass Spectrom. Ion Processes* **1990**, *100*, 209−265. Hoaglund, C. S.; Valentine, S. J.; Clemmer, D. E. *Anal. Chem*. **1997**, *69*, 4156−4161.

(30) The following examples illustrate current progress in IMS technology development: Hagen, D. F. *Anal. Chem.* **1979**, *51*, 870−874. Hill, H. H.; Siems, W. F.; St. Louis, R. H.; McMinn, D. G. *Anal. Chem.* **1990**, *62*, A1201−A1209. St. Louis, R. H.; Hill, H. H. *Crit. Rev. Anal. Chem.* **1990**, *21*, 321−355. von Helden, G.; Hsu, M.-T.; Kemper, P. R.; Bowers, M. T. *J. Chem. Phys.* **1991**, *95*, 3835−3837. Jarrold, M. F. *J. Phys. Chem.* **1995**, *99*, 11−21. Clemmer, D. E.; Jarrold, M. F. *J. Mass Spectrom.* **1997**, *32*, 577−592.

(31) Relevant sources describing computational approaches and structural information obtained from IMS: Jarrold, M. F.; Constant, V. A. *Phys. Rev. Lett.* **1991**, *67*, 2994−2997. Wyttenbach, T.; von Helden, G.; Batka, J. J., Jr.; Carlat, D.; Bowers, M. T. *J. Am. Soc. Mass Spectrom.* **1997**, *8*, 275−282. Mesleh, M. F.; Hunter, J. M.; Shvartsburg, A. A.; Schatz, G. C.; Jarrold, M. F. *J. Phys. Chem.* **1996**, *100*, 16082−16086. Shvartsburg, A. A.; Jarrold, M. F. *Chem. Phys. Lett.* **1996**, *261*, 86−91.

(32) Jarrold, M. F.; Bower, J. E.; Creegan, K. *J. Chem. Phys.* **1989**, *90*, 3615−3628. von Helden, G.; Wyttenbach, T.; Bowers, M. T. *Science* **1995**, *267*, 1483−1485. Gidden, J.; Wyttenbach, T.; Batka, J. J.; Weis, P.; Jackson, A. T.; Scrivens, J. H.; Bowers, M. T. *J. Am. Chem. Soc.* **1999**, *121*, 1421−1422. Gidden, J.; Wyttenbach, T.; Batka, J. J.; Weis, P.; Jackson, A. T.; Scrivens, J. H.; Bowers, M. T. *J. Am. Soc. Mass. Spectrom.* **1999**, *10*, 883−895. Hoaglund Hyzer, C. S.; Counterman, A. E.; Clemmer, D. E. *Chem. Rev.* **1999**, *99*, 3037−3079.

(33) See the following and references therein: Collins, D. C.; Lee, M. L. *Anal. Bioanal. Chem.* **2002**, *372*, 66−73. Wyttenbach, T.; Bowers, M. T. *Top. Curr. Chem.* **2003**, *225*, 207−232. Creaser, C. S.; Griffiths, J. R.; Bramwell, C. J.; Noreen, S.; Hill, C. A.; Thomas, C. L. P. *Analyst* **2004**, *129*, 984−994. McLean, J. A.; Ruotolo, B. T.; Gillig, K. J.; Russell, D. H. *Int. J. Mass Spectrom*. **2005**, *240*, 301−315. Tang, K. Q.; Li, F. M.; Shvartsburg, A. A.; Strittmatter, E. F.; Smith, R. D. *Anal. Chem*. **2005**, *77*, 6381−6388.

(34) Hoaglund, C. S.; Valentine, S. J.; Sporleder, C. R.; Reilly, J. P.; Clemmer, D. E. *Anal. Chem.* **1998**, *70*, 2236−2242. Counterman, A. E.; Valentine, S. J.; Srebalus, C. A.; Henderson, S. C.; Hoaglund, C. S.; Clemmer, D. E. *J. Am. Soc. Mass Spectrom.* **1998**, *9*, 743−759. Srebalus Barnes, C. A.; Clemmer, D. E. *Anal. Chem.* **2001**, *73*, 424−433. Liu, X.; Valentine, S. J.; Plasencia, M. D.; Trimpin, S.; Naylor, S.; Clemmer, D. E. *J. Am. Soc. Mass Spectrom.* **2007**, *18*, 1249−1264.

(35) Tang, K.; Shvartsburg, A. A.; Lee, H.; Prior, D. C.; Buschbach, M. A.; Li, F.; Tolmachev, A. V.; Anderson, G. A.; Smith, R. D. *Anal. Chem*. **2005**, *77*, 3330−3339.

Ion Gating. Ions can be gated at several locations in the instrument. The first gate, located at the exit of F1, is used to initiate ion mobility measurements. Accumulated ions are released by lowering a repulsive field thus transmitting ions through G1. G2 is located at the entrance to F2 and serves to gate ions of a particular mobility into the remaining portion of the instrument. For the present study, this gate is operated in transmission mode, except for collision cross section determination. In this case, the repulsive field is lowered at a predefined time (t_{delay}) with respect to G1. Scanning this delay time across the ion distribution until the peak maximum is located allows us to determine the drift times for ions through the D1 region. The trap, release, delay, and gating system associated with the G1 and G2 regions is controlled by a pulse delay generator (model DG535, Stanford Research Systems, Inc., Sunnyvale, CA) and occurs at a defined time after the initial drift pulse.

Determination of *m/z* Values. Ions exit the drift tube through an interface region and are focused into the source region of an orthogonal reflectron TOF mass spectrometer as described elsewhere.[34]

Determination of Experimental Cross Sections. Collision cross sections are determined from the relation[36]

$$\Omega = \frac{(18\pi)^{1/2}}{16}\frac{ze}{(k_bT)^{1/2}}\left[\frac{1}{m_I}+\frac{1}{m_B}\right]^{1/2}\frac{t_dE}{L}\frac{760}{P}\frac{T}{273.2}\frac{1}{N}$$

where t_d, E, and L are the drift time, electric field, and drift length, respectively, for the region of interest; T and P are the temperatureand pressure of the buffer gas, respectively; ze is the ion's charge; k_b is Boltzmann's constant; m_I and m_B are masses of the ion and buffer gas, respectively; and N is the neutral number density. In the present work, all cross sections are determined from the position of a peak as determined by scanning t_{delay} across the narrow region associated with the peak. Because this time corresponds only to the time spent in the uniform field drift region, and because there are no penetration effects associated with ion injection or end effects associated with removal of ions from the drift region, this is an extremely accurate and precise approach for determining cross sections. Any two measurements of the same system usually agree to within 0.5% relative uncertainty.

Molecular Modeling and Cross Section Calculations. Molecular modeling techniques and cross section calculations were used for several trial geometries of two PEG sizes coordinated to Cs^+ ions ($[HO(CH_2CH_2O)_xH + Cs]^+$; $x = 30$, $n = 2,3$ and $x = 126$, $n = 9$) in order to gain some insight about ion structure and trends associated with varying the number of charges. Trial geometries were constructed in the Insight II (Accelrys Inc., San Diego, CA, 2002) modeling environment that maximized the number of Cs^+ ions coordinated to oxygen atoms on the PEG backbone and differed in geometry from compact globules to more extended linear structures. Molecular dynamics of initial structures were performed at 300 K for a period of 100 ps, sampled periodically, and minimized using the extensible systematic force field (ESFF)[37] in order to generate trial structures for cross section calculations. Trajectory collision cross sections were then calculated for the ESFF optimized structures using the MOBCAL program (Indiana University, Bloomington, IN), developed by Jarrold and co-workers,[38] and compared to experimentally determined cross sections.

Nomenclature. In the present paper, we describe peak positions for nested drift(flight time) data using the nomenclature proposed previously in units of $t_d(m/z)$, where the value of t_d is given in milliseconds.[18,34]

Materials and Sample Preparation. PEG samples [weight average molecular weight (M_w) = 6550; number average molecular weight (M_n) = 6170; PDI) =1.03; and M_w=17 900, M_n = 14 900; PDI = 1.20) (Polymer Standards Services, Mainz, Germany)] in 50:50 water/acetonitrile solution, containing 1 M cesium acetate (Sigma-Aldrich, St. Louis, MO) and 1 M CsCl (Sigma-Aldrich), were used for these studies. The PEG 6550 and 17 900 sample concentrations were 0.25 and 1.0 mg mL^{-1}, respectively, which changed the relative amount of salt present and reduced background.

Data Acquisition and Processing. A robotic nanoflow ion source NanoMate HD autosampling system (NanoMate, Advion BioSciences, Inc., Ithaca, NY) was used for sample introduction with acquisitions between 5 and 20 min. Slicing software written in-house was used and the Origin software 6.1 and 7.0 (OriginLab Corp., Northampton, MA 01060) was employed for the three-dimensional plots.

RESULTS AND DISCUSSION

Nested IMS−MS Distributions for PEG 6550. Figure 2 shows drift time and m/z distributions for the PEG 6550 sample measured using the 3-m drift tube in transmission mode. The majority of signals associated with PEG appear along several narrow regions of the two-dimensional data set. Examination of the complete distribution (Figure 2A) shows at least two resolvable families: a group of peaks that extends from $t_d(m/z)$ ~32(550) to 45(850) and a second group from $t_d(m/z)$ ~ 42(700) to 57(1100).

It is interesting to examine a region of this data set over a narrower range that includes both of these groups of ions. Figure 2B shows an inset of the region $t_d(m/z)$ ~39(700) to 51(850). This enlargement of the data set has a somewhat striking visual pattern. Some insight into the pattern of peaks comes from taking diagonal slices through the data that can be used to obtain mass spectra over this range. Ten such slices are shown in Figure 3 for the 700 to 850 m/z range of this PEG sample (repeat unit 44 Da). The difference of 22 in m/z of peaks associated with slice 1 allows us to immediately identify this set of peaks as the +2 charge state of a series of cesiated PEG oligomers {i.e., $[HO(CH_2CH_2O)_xH + nCs]^{n+}$, where $x = 26$ to 30}. Similarly, slice 2 corresponds to a series having $n = 3$ and $x = 39$ to 48; slice 3 corresponds to $x = 4$ and $m = 52$ to 63, and so on. That is, we have resolved ions into individual charge states, as has been done previously for other systems.[15]

What makes this data set remarkable and visually striking is that the charge states can be resolved to essentially baseline of the entire PEG 6550 sample (previously characterized by bulk

(36) Mason, E. A.; McDaniel, E. W. *Transport Properties of Ions in Gases*; Wiley: New York, 1988.
(37) Shi, S.; Yan, L.; Yang, Y.; Fisher-Shaulsky, J.; Thacher, T. *J. Comp. Chem.* **2003**, *24*, 1059−1076.
(38) Mesleh, M. F.; Hunter, J. M.; Shvartsburg, A. A.; Schatz, G. C.; Jarrold, M. F. *J. Phys. Chem.* **1996**, *100*, 16082−16086. Shvartsburg, A. A.; Jarrold, M. F. *Chem. Phys. Lett.* **1996**, *261*, 86−91. http://nano.chem.indiana.edu/Software.html.

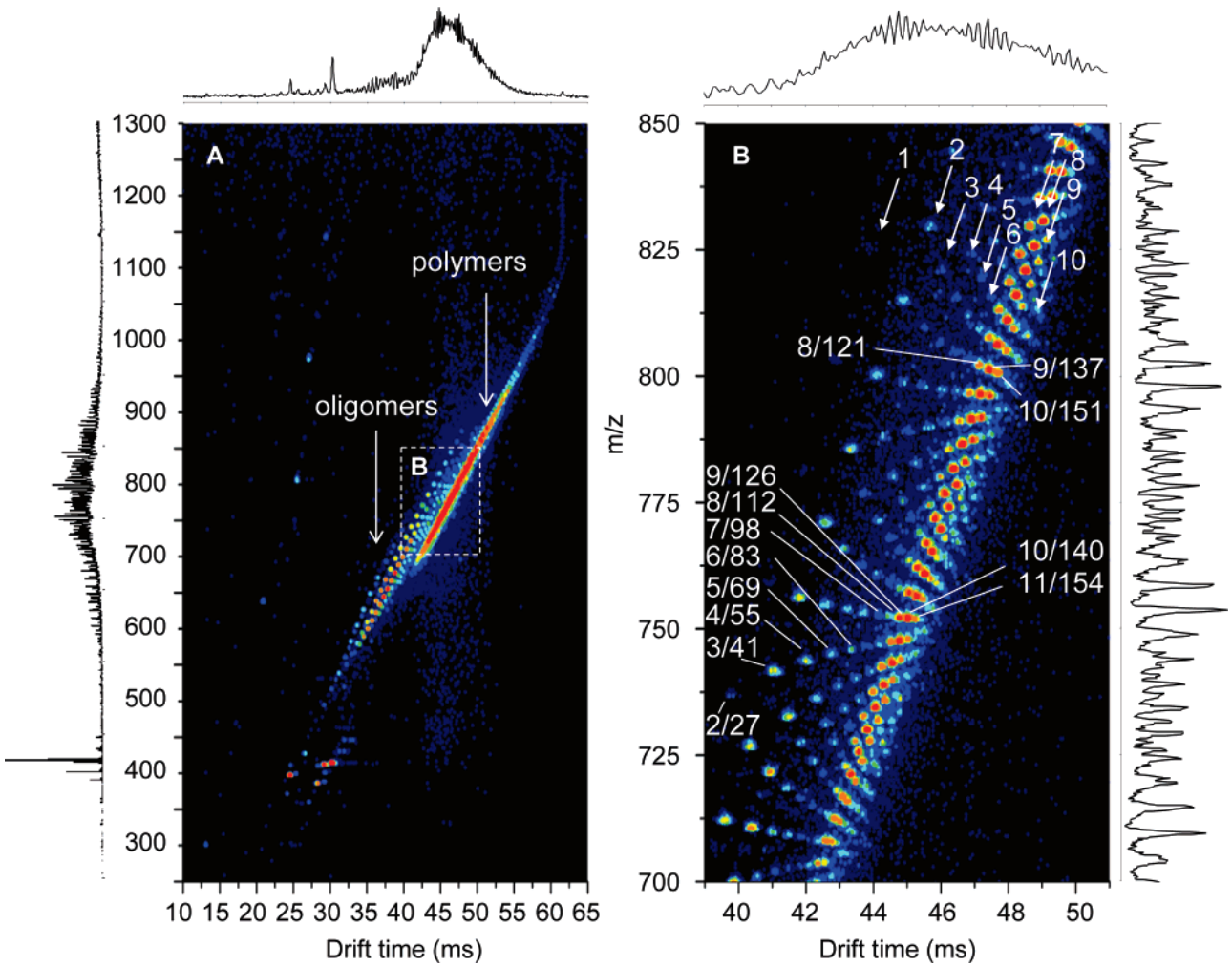

Figure 2. Two-dimensional $t_D(m/z)$ distribution of PEG 6550 doped with cesium acetate. The $t_D(m/z)$ distribution is shown on the left (inset A) with the integrated mass spectrum (trace on left of inset A) and integrated drift time distribution (top trace on inset A). The groups in the distribution corresponding to oligomers and polymers are labeled. Inset B (right panel) shows an expanded view of the $t_D(m/z)$ region of the most intense polymer features with representative integrated drift time distribution and mass spectrum. The charge-state resolved components are labeled by charge-state families ranging from low-intensity +2 oligomers to the more intense +10 and +11 polymers (white arrows).

methods; see Materials and Sample Preparation), even as we reach individual polymer chain lengths approaching those of $n = 10$, $x = 129$ to 162 and $n = 11$, $x = 152$ to 156, permitting end-group analysis [$R_1(CH_2CH_2O)_xR_2$, with R_1= OH and R_2 = H]. Additionally, the appearance of Figure 2B is influenced by the relative intensities of different polymer sizes. That is, the majority of ion intensity is associated with the expected polymer. However, there is another distribution that is concentrated around the $x = 30$ to 50 size range. This size range is most intense for the $n = 3$ family. Thus, the appearance of Figure 2A results from at least two distributions of ions: oligomers that center around 37(670) and may persist to as large as $x \sim 100$ and a more fully grown set of polymers that center around 47(800) and begin showing up as peaks with increasing intensity at $x = \sim 110$ in the $n = 8$ family. The most intense regions of the polymer distribution appear in the $n = 9$ family for $x = 135$ to 145.

Evidence for multiple distributions (oligomers and polymers)[39] in this system is remarkable. Integrating the peak area corresponding to the polymers in the two-dimensional data set provides a drift time distribution that reflects only the polymer ionsdetected; the obtained value estimates the polymers to be ~75% of the total drift time distribution of the PEG 6550 sample. The species may have different ionization efficiencies similar to observations from analysis by MALDI.[8] PEG is synthesized traditionally by anionic polymerization; this would lead to the conclusion of early termination of the growing polymer chain. Two size families are distinguishable using IMS−MS polymer characterization (including end-group determination for all charge states). The determination of the bulk property may likely be improved (such problems using MS analysis associated with broad PDI);[2,8] the success may be related to the metal cation−polymer interrelationship.

(39) IUPAC. *Polymer*: A molecule of high relative molecular mass, the structure of which essentially comprises the multiple repetition of units derived, actually or conceptually, from molecules of low relative molecular mass. Notes: In many cases, especially for synthetic polymers, a molecule can be regarded as having a high relative molecular mass if the addition or removal of one or a few of the units has a negligible effect on the molecular properties. *Oligomer*: A molecule of intermediate relative molecular mass, the structure of which essentially comprises a small plurality of units derived, actually or conceptually, from molecules of lower relative molecular mass. Notes: A molecule is regarded as having an intermediate relative molecular mass if it has properties which do vary significantly with the removal of one or a few of the units.

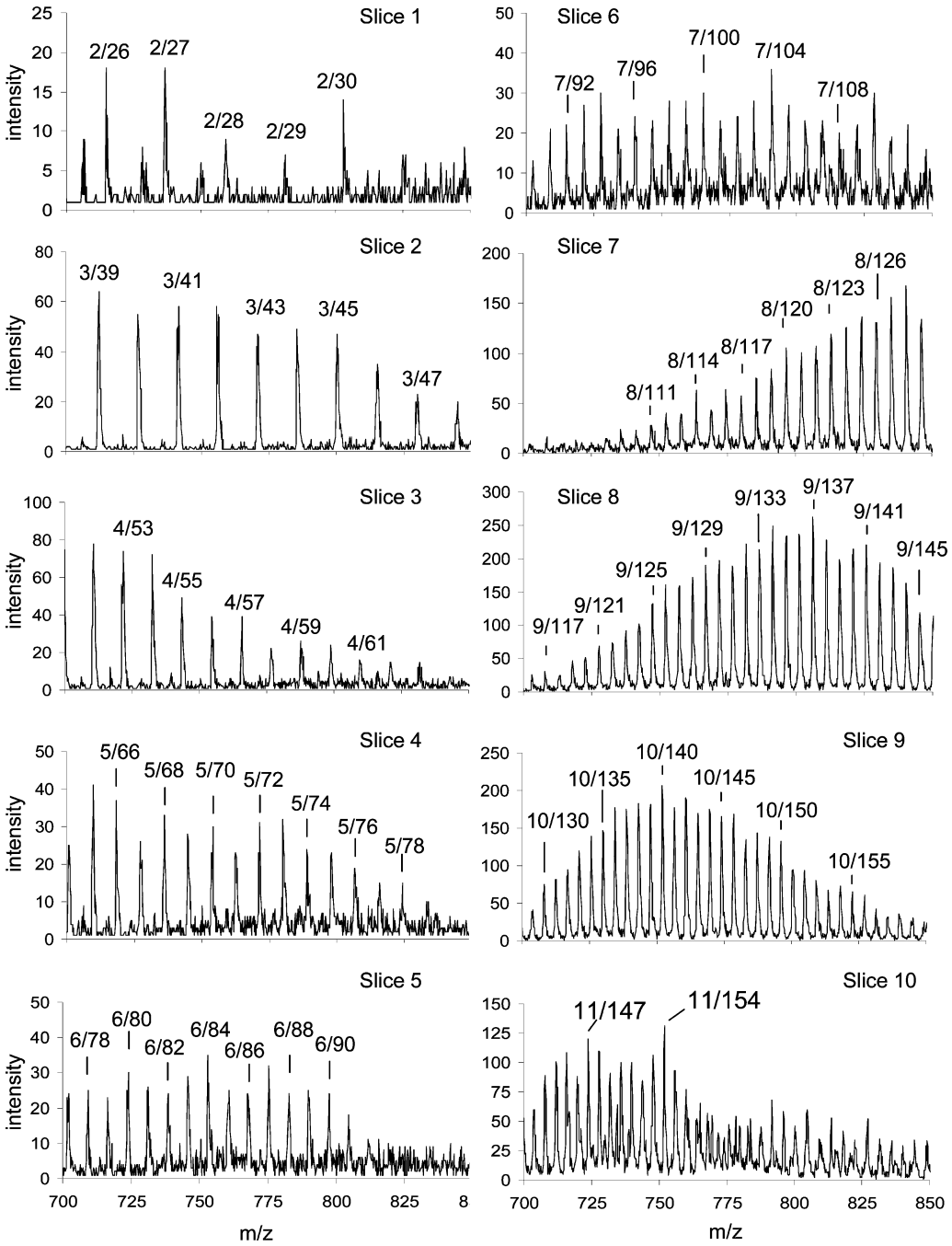

Figure 3. Mass spectra of several charge-state families from PEG 6550 doped with cesium acetate. The mass spectrum obtained by integration along a diagonal in the $t_D(m/z)$ distribution is used to generate slices in the m/z dimension for charge-state families ranging from the +2 series (slice 1) to the +11 series (slice 10). Prominent features in the charge-state resolved mass spectra are labeled by charge state/PEG residue number.

Nested IMS−MS Distributions for PEG 17 900. Figure 4 shows the drift time and m/z distributions for the PEG 17 900 sample acquired using the 2-m drift tube in transmission mode (60-V activation at F2). The majority of signals associated with PEG again show at least two resolvable families in the two-dimensional data set. One group of peaks extends from $t_d(m/z) \sim 23(780)$ to 32(1075) (Figure 5) and a second group from $t_d(m/z) \sim 16(550)$ to 23(850); both these groups somewhat overlap in their outer bounds. As expected, the chemical background is large for this higher molecular weight sample; the total mass spectrum (Figure 4) and drift time distributions of PEG 17 900 are dominated by Cs salt-related signals.

Figure 5 shows an inset of the region $t_d(m/z) \sim 21(790)$ to 27.5(890). Some insight into the pattern of peaks of this higher molecular weight PEG 17 900 sample can be obtained from taking diagonal slices through the data providing its respective mass spectra over the selected range. Our interest was captured by the red, thus, most intense feature within the polymer group, $t_d(m/z) \sim 23(780)$ to 32(1075). A representative slice is shown in Figure 5 for the 775 to 1075 m/z range extracting the entire length of the polymer body to the left side of the extended feature. The difference of the peaks with the two highest intensities (m/z 836.42 and 838.47) in the mass spectrum associated with slice P1 allows us to determine this set of peaks as the +22 with [HO(CH_2-

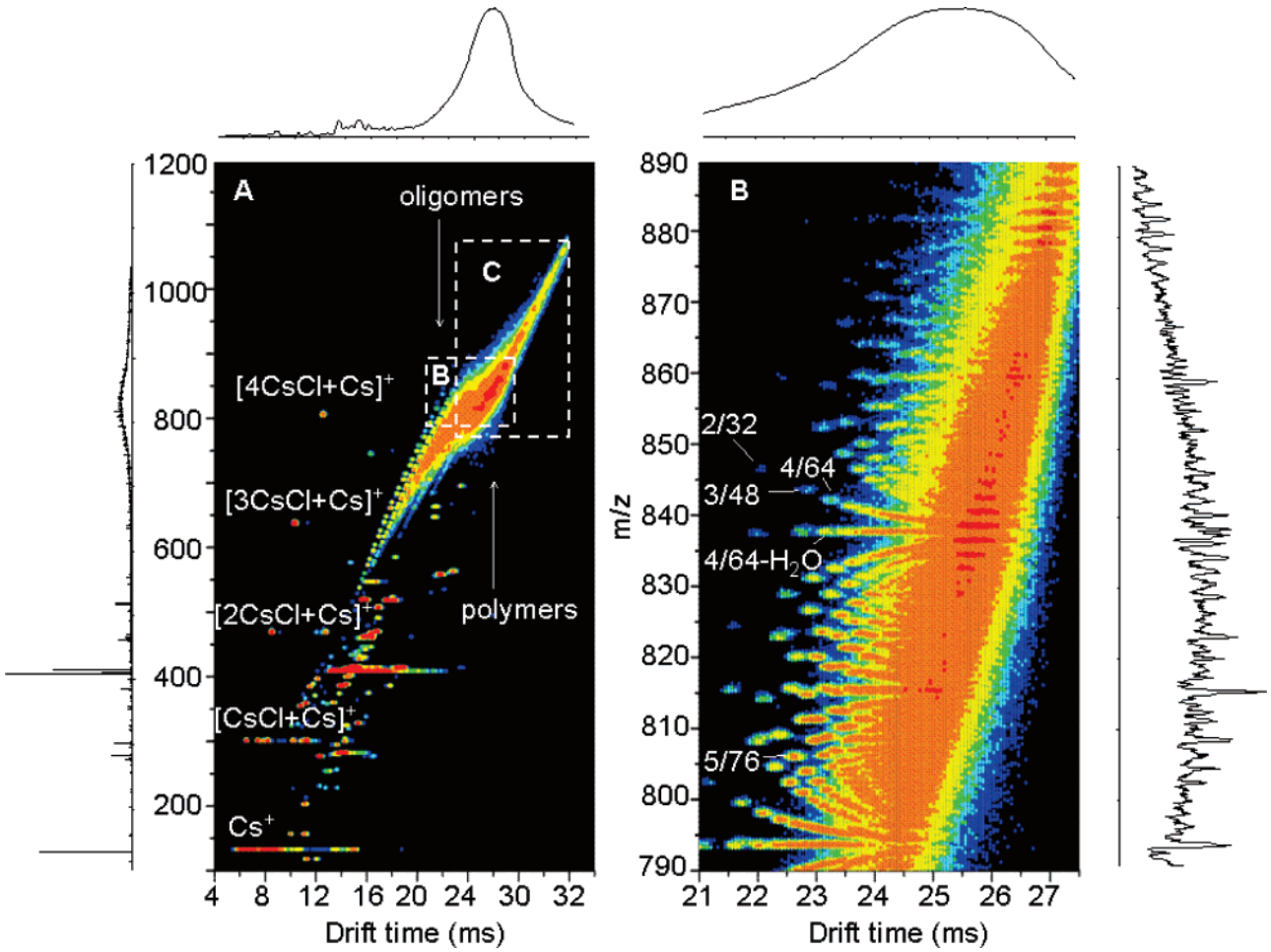

Figure 4. Two-dimensional $t_D(m/z)$ distribution of PEG 17 900 doped with cesium chloride. The $t_D(m/z)$ distribution is shown on the left (inset A) with corresponding total drift time distributions and integrated mass spectrum (top and leftmost trace, respectively). Prominent features in the distribution include cesium chloride clusters and regions dominated by oligomers and polymers (C, see Figure 5). Inset B shows an expanded view of the $t_D(m/z)$ region where the representative polymer (high charge-state) family is separated from smaller species (oligomers).

$CH_2O)_xH + 22Cs]^{22+}$, $x = 351$ and 352. Charge state of a series of cesiated PEG oligomers {i.e., $[HO(CH_2CH_2O)_xH + 22Cs]^{22+}$, where $x = 348$ to 357} can be assigned this way until the point in the spectrum where peaks overlap with the next charge states. In a similar fashion, peak series within charge states $n = 17$ to 23 have been assigned. We have partially resolved ions into individual charge states, which has been accomplished previously only by using high-resolution FT-MS analysis.[14]

Analogous to PEG 6550, low molecular weight oligomers were again observed for PEG 17 900 even though this is a polymer with a narrow polydispersity. Again, charge-state families +2 through +7 are determined within the feature assigned as oligomers. There is no evidence that these are fragment ions; therefore, the assumption is that we are detecting these low-mass components due to the IMS separation. Gel-permeation chromatography did not provide evidence for low molecular weight components.[40] In the low-mass region, however, this complementary method detects only those contaminants at abundances of >5%; discrepancies in results for GPC and MS attained polymer characterization have been described.[8] Consequently, the IMS approach, in addition to analyzing the higher molecular weight components, allows the detection of low-abundant components with high sensitivity.

(40) Personal communication with Dr. T. Hofe (Polymer Standards Service, Mainz, Germany).

General Trends Associated with Size and Charge-State Distributions. The analyses of both PEG 6550 samples leads to several interesting trends related to the size and charge-state distributions. The experimental data were acquired on the 2-m drift tube IMS instrument under low field conditions. Table 1 provides a summary of the range of sizes over which different numbers of Cs^+ ions are incorporated. These data were obtained by examining several data sets recorded for the two different samples on two different instruments and therefore reflect a general result for each set of sizes and charge states.

Examination of these data indicates that, in order to incorporate an additional Cs^+, thus leading to the next charge state, the polymer must be at least a minimum length. Presumably, the polymer must be large enough to stabilize the increase in repulsive Coulomb interactions that arise from inclusion of an additional charge. On average, and for several different analyses on different instruments, we find that ~10 ethylene oxide units are required to incorporate an additional Cs^+. This is an interesting value as it is similar to the coordination number of 10−11 reported by Wyttenbach et al.[20] for small oligomers ($x = 9$, 13, 17) associating with Cs^+.

If one assumes that the Cs^+ ions are highly coordinated and that this is essentially an upper limit of the coordination number, then the range of polymer sizes associated with a charge state

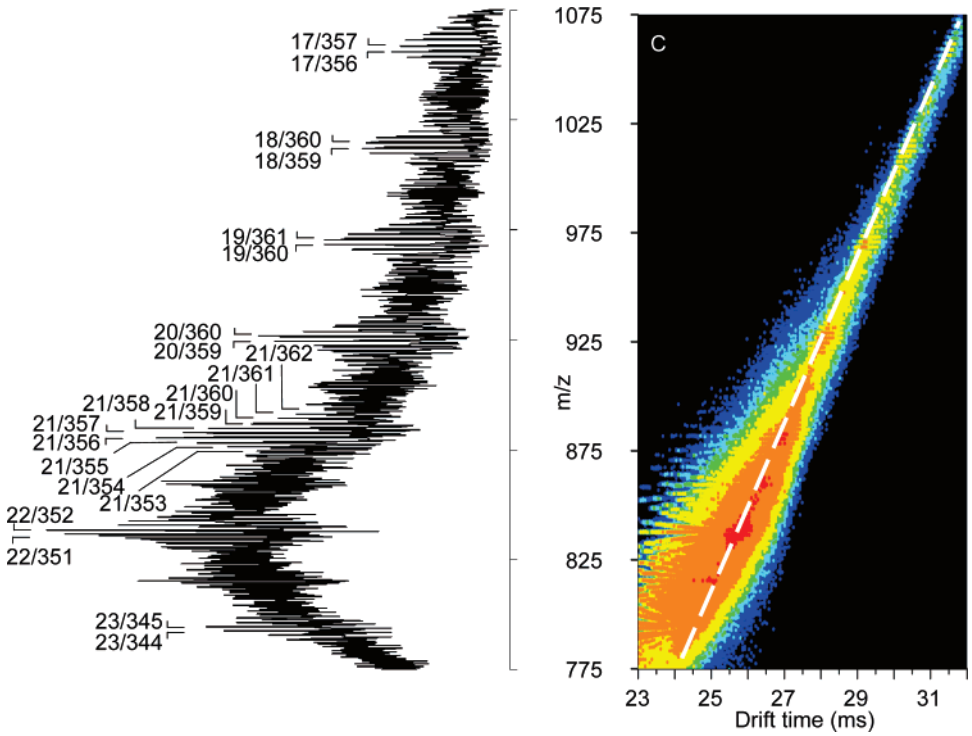

Figure 5. Expanded $t_D(m/z)$ distribution PEG 17 900 doped with cesium chloride corresponding to region C in Figure 4 shown on the right. Integration of a narrow region of drift times along the diagonal (dashed white line) of the $t_D(m/z)$ distribution was performed in order to obtain the mass spectrum shown on the left. The mass spectrum obtained from the diagonal slice shows the relative intensities of highly charged species with prominent features labeled by the number of incorporated cesium ions and the number of PEG units of polymer.

Table 1. Molecular Weights of the PEG Polymer within Each Slice Providing End-Group Analysis and Minimum and Maximum Numbers of PEG Repeats That Attach with Respective Numbers of Cesium Cations

		lower bound of the polymer distribution				upper bound of the polymer distribution			
no. slice	charge state[a]	m/z[b]	Da	no. × repeat units	× repeats per Cs^+	m/z[b]	Da	no. × repeat units	× repeats per Cs+
1	+2	604.11	942.22	20.99	10.5	780.31	1294.62	28.99	14.5
2	+3	535.11	1206.33	26.99	9	755.9	1868.7	42.03	14.01
3	+4	566.94	1735.76	39.01	9.75	764.76	2527.04	56.98	14.25
4	+5	603.32	2351.6	53	10.6	762.1	3145.5	71.03	14.21
5	+6	627.88	2969.28	67.03	11.17	760.15	3762.9	85.05	14.18
6	+7	645.07	3584.49	81	11.57	764.67	4421.69	100.02	14.29
7	+8	683.17	4402.16	99.52	12.44	817.92	5480.16	123.99	15.5
	+9	717.35	5260.05	119	13.22	815.16	6140.34	138.98	15.44
	+10	680.98	5480.8	124.01	12.4	742.53	6096.3	137.98	13.8
8	+9	761.39	5656.41	127.99	14.22	824.92	6228.18	140.97	15.66
	+10	716.15	5832.5	131.99	14	808.75	6758.5	153.01	15.3
	+11	683.17	6052.97	136.99	12.45	739.21	6669.41	150.99	13.73

[a] For baseline resolved results, view Figures 2 and 3. [b] *m/z* values were obtained from low field measurements on the 2-m drift tube IMS instrument. Signals present in the mass spectrum with intensities of about >10% parent ion were included to the table only. This assessment is equivocal for two reasons: the determination of the upper bound as the signal intensities faded slowly; for slices 7 and 8 signal overlaps of charge states make the determination of the upper and lower bound of a particular charge state inaccurate.

provides a feeling about the number of monomer units that would be expected to reside in between the coordinated Cs^+ sites. For example, $[HO(CH_2CH_2O)_xH + 3Cs]^{3+}$ ions exists from $x = 27$ to 42; for all three Cs^+ ions to remain highly coordinated in the smallest size $[HO(CH_2CH_2O)_{27}H + 3Cs]^{3+}$ species, essentially every monomer unit would need to be associated with at least one Cs^+. It seems likely that such small polymers may adopt lower coordination numbers in order to reduce the repulsive interactions between charges. The $[HO(CH_2CH_2O)_{42}H + 3Cs]^{3+}$ oligomer could adopt an average coordination number of 10 around all three charged sites and have 12 monomers to spare as linking domains, in this case, two linking regions each consisting of ~6 monomer units. As another example, consider the larger $[HO(CH_2CH_2O)_xH + 9Cs]^{9+}$ polymers, existing from $x = 128$ to 141; the size distribution for this charge state suggests that on average there are ~4−6 monomer units that link the charged solvated ion regions together. Of course, these arguments need to be somewhat flexible as changes in the coordination numbers will influence the average linker domain length.

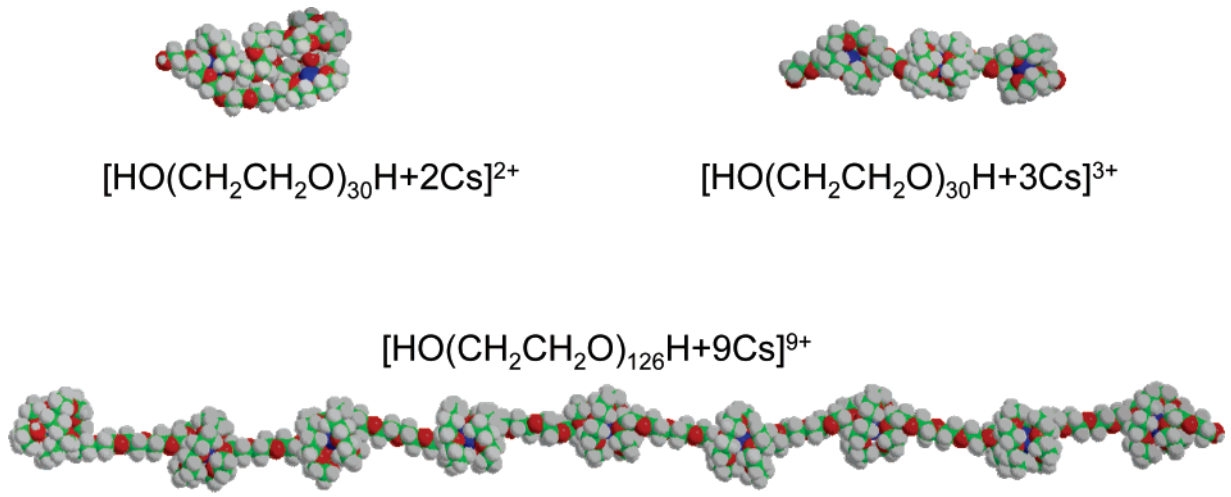

Figure 6. Representative ESFF minimized PEG structures obtained from molecular modeling. Representative structures of $[HO(CH_2CH_2O)_{30}H + xCs]^{x+}$ with $x = 2$ and $x = 3$ are shown at the top. The increase in Coulomb repulsion for the +3 charge state ($\Omega_{expt/calc}$ = 422.1 Å^2/407.4 Å^2) favors a more elongated state from a more compact state as in the +2 structure ($\Omega_{expt/calc}$ = 360.4 Å^2/348.2 Å^2). The optimized structure for $[HO(CH_2CH_2O)_{126}H + 9Cs]^{9+}$ minimizes Coulomb repulsion by adopting a fully extended conformation while keeping a high degree of coordination; good experimental agreement (Ω_{expt} = 1696.75 Å^2 ,Ω_{calc} 1661.8 ± 17.2 Å^2) is observed.

General Characterization of Structures for Oligomers and Polymers from Molecular Modeling. The structures of PEG ions have attracted considerable attention.[20−23] Relatively small singly charged PEGs (x = 9, 13, and 17 with several different cations including Li^+, Na^+, and Cs^+) appear to favor relatively compact conformations.[20] A general feature of these ions is that those such as Cs^+ are highly coordinated. Larger multiply charged PEG ions produced by ESI have also attracted some attention. De la Mora and co-workers[23] have argued that ions favor a range of conformations, from those that are highly spherical to those that are extremely linear; the transition from compact to linear occurs with increasing charge and is thus driven by the total Coulomb energy associated with the highly charged ions in the dielectric of the vacuum.

Here we focus on two size regimes that are important for the separation of oligomers from polymers that we observed in the PEG 6550 sample under low field conditions: an oligomer with x = 30 and n = 2 or 3 and a polymer with x = 126 and n = 9. We intend this discussion only as a treatment of the conformation that is useful for understanding the rather striking resolution of sizes and charge states that is observed.

Figure 6 shows several examples of structures. In general, the dynamics simulations reveal several trends. First, at 300 K the simulations indicate that ions are highly dynamic; as found previously for small PEG ions; oxygen atoms are closely coordinated with the Cs^+ charge site, such that the charge is highly solvated. The optimized geometry for $[HO(CH_2CH_2O)_{30}H + 2Cs]^{2+}$ showed a compact structure with a calculated cross section of 348 Å^2 (Ω_{expt} = 360 Å^2). As Cs^+ is added to the poly(ethylene oxide) chain (in comparing the x = 2 and x = 3), the polymer adopts a more extended conformation. This result is consistent with the lower mobility of the higher-charge-state family, as observed experimentally and results from an increase in the total Coulomb energy for this system, similar to previous reports for multiply charged protein ions.[41] Although extended, these species still show high-coordination numbers ranging from 7 to 9 around the charged sites. Thus, we refer to these structures as beads on a string. The calculated cross section for this geometry was 407 Å^2 and agreed with the experimentally determined cross section (Ω_{expt} = 422 Å^2).

We extended these ideas from the oligomers to the polymers by considering several different types of initial structures and the role of Coulomb repulsion for a system of charges on a string. In one series of models, we began by considering relatively random geometries such as those that might be expected in solution. For example, if we start with 9 Cs^+ sites on the surface of a sphere or in a higher energy configuration within a volume of a sphere, we then assembled the polymer chain (x = 126) around the charges. With this approach, it is possible to create individual charge sites that are highly coordinated (solvated) by different regions of the polymer chain. The resulting structures have interesting, globular appearances; however, in all of the cases that we examined, they are relatively high in energy and the calculated cross sections are far below any experimental values. When dynamics simulations are run on these ions, they rapidly open up. As the globular configurations approach extended conformations, the charge coordination switches from utilization of distant regions of the polymer chain to more localized charge solvation.

One final note of interest involves the issue of where 9 charges reside along a polymer containing 126 monomer units. We have tried several configurations for these studies. Ultimately, the lowest energy structures are those that reduce Coulomb interactions while retaining highly coordinated charge sites. In order to minimize Coulomb interactions, charges are not spaced equally along the polymer chain. Rather, these repulsive interactions are

(41) Valentine, S. J.; Anderson, J. G.; Ellington, A. D.; Clemmer, D. E. *J. Phys. Chem. B* **1997**, *101*, 3891−3900. Clemmer, D. E.; Hudgins, R. R.; Jarrold, M. F. *J. Am. Chem. Soc.* **1995**, *117*, 10141−10142. Shelimov, K. B.; Clemmer, D. E.; Hudgins, R. R.; Jarrold, M. F. *J. Am. Chem. Soc.* **1997**, *119*, 2240−2248. Covey, T. R.; Douglas, D. J. *J. Am. Soc. Mass Spectrom.* **1993**, *4*, 616−623.

minimized by localizing charges near the poly(ethylene oxide) chain starting at positions corresponding to 1, 16, 30, 44, 57, 72, 86, 101, and 115; in one simulation numbers between 9 and 10 (i.e., distances between $Cs^+-O < 4$ Å). The calculated trajectory cross section for this type of geometry is 1661 $Å^2$ and agrees within 2% of the experimentally determined cross section ($\Omega_{expt} = 1697$ $Å^2$). Overall, such a structure is basically consistent with the earlier work on coordination numbers by Wyttenbach et al.[20] and is also consistent with the linear geometry proposed by de la Mora.[23] That is, locally charged sites are highly coordinated, while globally the geometry is highly extended.

CONCLUSIONS

ESI-IMS−MS has been used to examine synthetic polymers, PEG 6550 and 17 900. The introduction of a mobility separation prior to MS results in a significant reduction in spectral congestion as compared to ESI-MS alone and allows many features associated with a range of different sizes and charge states to be resolved. Of interest in the present work is that the mobilities of families of different charge states decrease with increasing charge. This is an indication of substantial transitions in structure. In this case, addition of charges increases the Coulomb energy, causing ions to expand with increasing charge. Comparisons of experimental cross sections with those that are calculated for trial conformations generated by molecular modeling indicate that the high-charge states adopt open conformations that are highly dynamic. It appears that in many cases nearly linear conformations that distribute charges in a low-energy configuration are favored. The Cs^+ ions themselves still appear to be highly coordinated by oxygen atoms of the ethylene oxide repeat unit as is observed from studies of smaller singly cesiated ions.

Traditionally, synthetic polymers are characterized by a number of techniques that provide information, albeit indirect, about the sample as a bulk system; these approaches are also relatively insensitive. Thus, it is difficult to pick up on small impurities, such as the distribution of oligomers that are observed in the PEG 6550 and 17900 sample. Techniques such as MALDI-MS,[2,7,8] in particular hyphenated liquid chromatography-MALDI methods,[9] are beginning to provide additional insight about the complexity associated with these samples, and as we have reported, ESI-MS[10] shows promise, with the limitation that size distribution information is complicated because it is convoluted over different charge-state distributions for different sizes. Inclusion of an IMS dimension provides a relatively simple solution and effectively no additional time for total analysis.

We anticipate that the approach will have value in the analysis of other types of polymers, for example: copolymers, amenable to ESI analysis, some of which are still only tractable for analysis with techniques such as gel-permeation chromatography, nuclear magnetic resonance spectroscopy, and high-resolution FT-MS methods. Additionally, it would be interesting to combine other ionization sources with IMS−MS analysis, as it is likely that this will improve the types of observable ions.

ACKNOWLEDGMENT

The authors are grateful for financial support from the Indiana METACyt Initiative (funded by the Lilly Endowment). S.T. thanks Dr. Thorsten Hofe (Polymer Standard Services, Mainz, Germany) for the generous donation of samples.

Received for review July 25, 2007. Accepted August 29, 2007.

AC071575I